JOURNAL OF SPACECRAFT AND ROCKETS
Vol. 31, No. 4, July–August 1994

Integrated Inlets for Cone-Derived Waveriders with Combined Transverse and Longitudinal Curvature

Sheam-Chyun Lin* and Yu-Shan Luo†
National Taiwan Institute of Technology, Taipei, Taiwan 10772, Republic of China

A generic aerospace vehicle is constituted of three parts: a forebody, a scramjet, and an afterbody. This paper is concerned with the design of the forebody and the inlet by means of waverider configurations. Hypersonic stream surfaces past a cone with combined transverse and longitudinal curvature are used to design integrated inlets for waveriders. By suitably choosing a second-order even polynomial stream surface, inlet shapes can be controlled. Mass flow rate, wetted surface area, volume, lift, drag, and lift-to-drag ratio can be found in closed forms. Effects of various parameters on the shape of the inlet are found and discussed in detail. Thus, an overall aerodynamic design of a hypersonic vehicle can be established in a simple and systematic way. Flight conditions are determined for a wide range of shapes and parameters as well as other related factors depending on the designer's interest.

Nomenclature

G_{mn} = shock-perturbation factor
ℓ = length of right circular cone
ℓ_w = length of waverider
q = dynamic pressure, $\rho_\infty V_\infty^2/2$
R = distance quantities, $r\theta/\ell\delta$
r, θ, ϕ = spherical coordinate system
U, V, W = spherical velocity perturbation components associated with curvature
u, v, w = velocity components in spherical coordinates
X, Y = nondimensional Cartesian coordinate system, $x/\ell\delta$, $y/\ell\delta$
x, y, z = Cartesian coordinate system
β = semivertex angle of the unperturbed shock
δ = semivertex angle of the unperturbed cone body
ϵ = perturbation parameter (define extremely small)
σ = ratio of shock angle to cone semi-vertex angle, β/δ

Superscript

* = quantities proposed in Ref. 5

Subscripts

c = compression surface quantities
f = freestream surface quantities
i = inlet surface quantities
ℓ = shock wave in base plane
m = mth term in expansion
n = nth term in expansion
s = shock wave
0 = zero-order, unperturbed flow quantities
∞ = freestream condition

Introduction

RECENTLY, because of the need for high-performance missiles and aircraft, design of hypersonic configurations which maximize aerodynamic performance has received increasing attention. Future high-speed lifting configurations must acquire the desirable properties of high-lift force, low-drag force, and high-volumetric efficiency. Kuchemann[1] gave a detailed discussion of modern hypersonic aircraft needs and their design problems. He recommended the use of stream surfaces of known flowfields as solid surfaces in a lifting-body configuration.

In principle, one possible approach for studying the aerodynamics of high-lift bodies is by means of a waverider concept. The aerodynamic advantage of the waverider is that the high pressure behind the shock wave under the vehicle does not "leak" around the leading edge to the top surface, such that the lift-to-drag ratio (L/D) for the waverider is considerably higher than that for the conventional aerodynamic vehicle. In addition to the superior aerodynamics of a forebody compression surface, it also provides favorable conditions for the flow at the engine inlet. This condition simplifies the design of inlets for scramjets.

The first study of waveriders was published in 1959 by Nonweilier,[2] who generated caret waveriders from the two-dimensional flowfield behind a plane oblique shock associated with a wedge. A well-known "exact" solution exists to the problem of steady supersonic flow past a right circular cone at zero incidence, commonly referred to as the Taylor-Maccoll[3] solution. Rasmussen[4] has proposed new waverider configurations derived from elliptic-cone stream surfaces according to the Taylor-Maccoll equation combined with the perturbation method.

Lin and Rasmussen[5] extended the waverider theory to take into account combinations of transverse and longitudinal curvature. Their approximate analytic solutions for the shock-layer flowfield are derived within the framework of hypersonic small-disturbance theory. It was shown that the types of waverider shapes derived from the perturbed flowfields have the advantage of efficient volumetric packaging and enhanced L/D values. These provide a systematic means for studying more efficient volume distribution related to the packaging of guidance, propulsion, and payload units. More recently, by choosing a sixth-order even polynomial to describe the trailing-edge curve of a waverider, Rasmussen and He[6] established a more feasible way to construct and analyze the aerodynamics of waveriders derived from axisymmetric flows past circular cones.

Generally speaking, an aerospace vehicle contains three parts: a forebody, a propulsion unit scramjet, and an afterbody. The aforementioned works are concerned with only the forebody. Following the underlying principle used in the design of a waverider itself, Hemdan and Jischke[7] took the stream surface of the flowfield for the elliptic cone as a solid surface; assuming

Received Aug. 24, 1992; revision received Feb. 17, 1993; accepted for publication April 27, 1993.

*Associate Professor, Department of Mechanical Engineering. Member AIAA.

†Graduate Research Assistant, Department of Mechanical Engineering.

inviscid flow, these surfaces were used to design smooth blended inlets attached to the waverider configuration. Rasmussen and Stevens[8] also proposed a similar idea for the inlet design. However, both of these works were still far from practical application due to the lack of complete analytical analysis of aerodynamic parameters.

In this paper, integrated inlets are generated for cone-derived waveriders with combined transverse and longitudinal curvature. Also calculated are many aerodynamic effects of the various parameters on the shapes of the inlet. Here, for demonstration purposes, we use a zero-slope-edge polynomial together with the approximate analytic solution from Ref. 5 to generate forebody configurations. With the same approach, and by suitably choosing a second-order even polynomial inlet freestream surface, inlet compression surfaces can be found. The space, confined by the waverider compression surface and inlet compression surface, can be treated as a stream tube in which the inlet and scramjet are located. Also, there are an infinite number of possibilities of waverider design with an integrated inlet corresponding to various inlet freestream surfaces. Using the superposition method, the mass flow rate, wetted surface area, lift, drag, and lift-to-drag ratio can be found in closed form. Thus, an overall aerodynamic design of hypersonic vehicles is created in a simple and systematic way.

Forebody Configuration

As stated previously, utilization of the waverider concept is the focus of this study; thus, the waverider construction should be established before we proceed to the investigation of the integrated inlet. Here, the nonaxisymmetric supersonic flowfield with longitudinal curvature is used to generate waverider configurations based on the analytic approximate solutions for the shock-layer flowfields[5] as derived within the framework of hypersonic small-disturbance theory. In the following subsections, the shock-layer stream surface and the construction procedure for developing waverider configurations are stated.

Shock-Layer Stream Surfaces

To study the stream surfaces, streamline equations in the shock layer are required. These are given by

$$V \times ds = 0 \tag{1}$$

From Ref. 5 [Eq. (7c)], the Eq. (1) can be expanded in spherical coordinates

$$\frac{dr}{u_0(\theta_0)} = \frac{r d\theta_0}{v_0(\theta_0)} = \frac{r\theta_0 d\phi}{\epsilon(r/\ell)^m W_{mn}(\theta_0)\sin(n\phi)} \tag{2}$$

The first two members of Eq.(2), by using hypersonic small-disturbance theory, will lead to

$$r = r_s \exp\left[\int_\beta^{\theta_0} \frac{u_0(\theta_0)}{v_0(\theta_0)} d\theta_0\right] \tag{3}$$

or, in parametric form

$$r = r(\theta_0; r_s) \tag{4}$$

where r_s is the location on the shock where a shock-layer streamline begins. Equation (3) constitutes a family of stream surfaces delineated by different stream surfaces of the family.

The last two members of Eq. (2) can be written in variable-separated form which are then integrated from a point where $r = r_s$ and $\phi = \phi_s$ on the shock wave. We can also get another family of stream surfaces. Therefore, a streamline is obtained from the intersection of these two families of stream surfaces as

$$\frac{\theta_0}{\delta} = \left(1 + (\sigma^2 - 1)\left\{1 + \frac{m}{nA^*}\left(\frac{\ell}{r}\right)^m \ln\left[\frac{\tan(n\phi/2)}{\tan(n\phi_s/2)}\right]\right\}^{2/m}\right)^{1/2} \tag{5}$$

where

$$A^* = -\frac{\epsilon W_{mn}(\delta)}{V_\infty \delta} \tag{6}$$

and W_{mn} is the azimuthal component of velocity. Equation (5) describes a streamline in the parametric form

$$\theta_0 = f(r, \phi; \phi_s) \tag{7}$$

Here, $r = r_s$, $\theta_o = \beta$, and $\phi = \phi_s$ designate a point on the shock where a streamline begins. An arbitrary compression stream surface can be obtained by specifying the functional relation $r_s = r_s(\phi_s)$.

Construction Procedure of a Waverider

Reference 8 states that a nonconical waverider configuration can be constructed by specifying either the trailing edge of the compression surface in the base plane or by specifying the trailing edge of the freestream surface in the base plane. (The waveriders considered here all have upper surfaces parallel to the freestream.) Assume the curve for the compression trailing edge is specified. Then the shock-layer streamlines passing through this base curve can be traced upstream to where they intersect the conical shock (i.e., from point B to point C in Fig. 1). These streamlines lie in a stream surface that constitutes the compression surface of a new waverider configuration. The conical flowfield above the intersection line can now be discarded and replaced by a new freestream surface constructed by tracing undisturbed free streamlines downstream from the shock-intersection line (from point C to point A in Fig. 1). These streamlines constitute the new freestream surface of the waverider. This freestream surface intersects the base plane and forms a freestream trailing-edge curve. Thus, specifying the compression surface trailing-edge curve in the base plane automatically determines the freestream surface trailing edge in the base plane. The reverse process is also valid; and this reverse approach is more convenient for the purpose of this analysis.

We consider cones with small semivertex angles such that the nondimensional coordinate are $X = x/(\ell\delta)$ and $Y = y/(\ell\delta)$

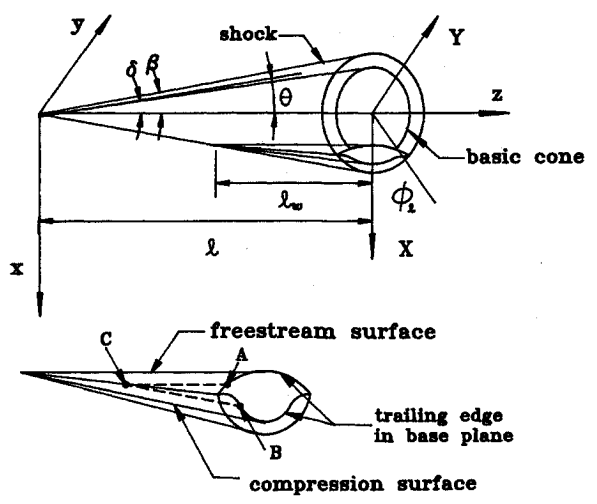

Fig. 1 Geometric configuration and coordinate system.

(see Fig. 2). The waverider freestream trailing-edge curve in the base plane is described by a function of the form $X = X(Y)$, which with some generality can be specified by the sixth-order even polynomial

$$X = R_0 + b_2 Y^2 + b_4 Y^4 + b_6 Y^6 \tag{8}$$

where R_0, b_2, b_4, and b_6 are coefficients to be specified. These four coefficients are determined by specifying four conditions that must be satisfied. We can find many families of conditions in Ref. 7. In this paper, a zero-slope-edge waverider is chosen as the forebody.

At this point, the freestream trailing-edge curve in X, Y coordinates can be rewritten in spherical coordinates as

$$X = R^*_{fb} \cos(\phi)$$
$$Y = R^*_{fb} \sin(\phi)$$

where

$$R^*_{fb} = (\theta)_{fb}/\delta$$

and so the polynomial becomes

$$R^*_{fb} \cos\phi = R_0 + b_2 R^{*2}_{fb} \sin^2\phi + b_4 R^{*4}_{fb} \sin^4\phi + b_6 R^{*6}_{fb} \sin^6\phi \tag{9}$$

By considering the coordinates proposed in Ref. 5, the relations between θ and θ_0 coordinates are

$$R_{fb} = 1 + (\sigma - 1)\left(\frac{R^*_{fb} - Z_1}{Z_2 - Z_1}\right) \tag{10}$$

and

$$R_{cb} = 1 + (\sigma - 1)\left(\frac{R^*_{cb} - Z_1}{Z_2 - Z_1}\right) \tag{11}$$

where

$$Z_2 = \sigma - \epsilon G_{mn} (r/\ell)^m \cos(n\phi)$$

$$Z_1 = 1 - \epsilon (r/\ell)^m \cos(n\phi)$$

R^*_{fb} and R^*_{cb} in Eqs. (10) and (11) represent displacements in the θ_0 coordinate. Extensive results for forebody generation can be found and discussed in detail in Ref. 9.

Integrated Inlets

Following the approach used to develop the waverider configuration for a forebody just discussed, the inlet will be constructed from the stream surface of the flowfield past a cone with combined transverse and longitudinal curvature. Also, air flowing through the stream tube, confined by waverider and inlet compression stream surfaces, will be the oncoming flow for the propulsion system. In this section, the shapes of waveriders with blended inlets are developed by using this characteristic.

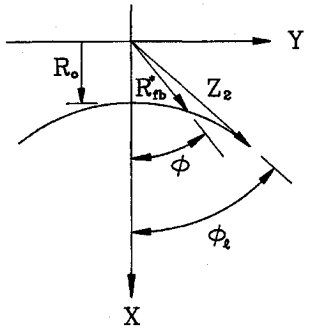

Fig. 2 Nondimensional coordinate system in the base plane.

Inlet Generation

Using a second-order even polynomial to specify the inlet freestream trailing-edge curve,

$$X = R_{i0} + b_{i2} Y^2 \tag{12}$$

the compression surface trailing-edge in the base plane is defined automatically. Equation (12) has only two coefficients to be determined. In addition, parameter ϕ_i is specified to control the width of inlet; thus there are three undetermined parameters.

To obtain the stream tube, both the waverider freestream trailing-edge curve and inlet freestream trailing-edge curve must pass through the same point (X_{ϕ_i}, Y_{ϕ_i}) when $\phi = \phi_i$. Therefore, the conditions

$$X_{w\phi_i} = X_{i\phi_i}$$
$$Y_{w\phi_i} = Y_{i\phi_i} \tag{13}$$

must be satisfied, where X_{ϕ_i} and Y_{ϕ_i} can be found in the freestream trailing-edge curve equation for a waverider. Thus

$$b_{i2} = (X_{\phi_i} - R_{i0})/Y^2_{\phi_i} \tag{14}$$

where subscripts w and i represent the properties of waverider and inlet, respectively.

Summarizing, only two variables, ϕ_i and R_{i0}, are needed to designate a particular freestream surface of an inlet. The compression surface of the inlet wall can be specified following the construction procedure for a waverider configuration. Figure 3 shows the position in which the inlet freestream and compression surface are located.

Inlet Length

Since the inlet length depends on the length of the propulsion unit, it is not necessary to take the whole inlet compression surface, from shock-intersection line to base plane, as the inlet wall. To control the inlet length, the fractional parameter (r_i/ℓ) is chosen in the following analyses. Physically speaking, the region $(r_i/\ell) \geq (r/\ell)$ is utilized as the actual inlet wall, whereas the front portion of the inlet compression surface is discarded. Moreover, there exist two geometric limitations for (r_i/ℓ) and R_0

$$R_{i0} \leq [\sigma - \epsilon G_{mn}(r_i/\ell)^m](r_i/\ell) \tag{15}$$

$$R_{i0} > R_0 \tag{16}$$

This implies that the whole inlet wall must be located inside the shock layer and under the waverider compression surface.

Mass Flow Rate of Inlet

Mass flow rate is an important parameter due to its direct relation to the thrust force of the propulsion unit. In principle, the mass flow rate will be given by

$$\text{mass flow rate} = \int\int \rho V \cdot d\mathbf{A} \tag{17}$$

As derived in Ref. 5, the analytic approximate expressions for density and velocity inside the shock layer are so complicated that the integration of Eq. (17) is intractable. To avoid this difficulty, a simple alternative is adopted in this paper. As discussed earlier, the inlet portion confined by the compression

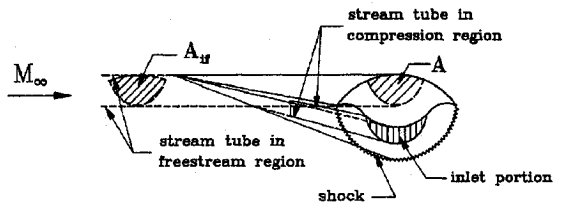

Fig. 3 Inlet stream tube side view.

stream surfaces of waverider and inlet wall can be treated as a stream tube, thus the mass flow rate of this stream tube is tantamount to the mass flow rate of the inlet. As a result of the definition of stream surfaces, the identical mass flow rate can be obtained in any cross section of this stream tube.

Obviously, the desirable location should be selected in a freestream region where the density and velocity are kept as constant values. To achieve this purpose, we extend this stream tube forward to where it intersects with the shock, and evaluate the mass flow rate over that particular cross section (see section A_{if} in Fig. 3). Therefore, the mass flow rate is easily obtained as the product of the cross-sectional area A_{if}, freestream density, and velocity

$$\text{mass flow rate} = \rho_\infty V_\infty A_{if} \tag{18}$$

Note that the direction of this cross-sectional area (A_{if}) is parallel with the freestream flowfield. Furthermore, according to the construction principle of waveriders,[10] the freestream and compression stream surfaces share the same leading edge, which is the intersection line of shock and stream tube; it follows that the lower curve of A_{if} can be replaced by the leading edge of the inlet freestream surface. Therefore, the projection of cross section A_{if} on the base plane will be the area A confined by the freestream trailing-edge curve of the waverider and the inlet as shown in Fig. 3.

In conclusion, with the aid of the freestream trailing-edge curve for the waverider and inlet, we can express the useful cross-sectional area of the stream tube as

$$A = A_{if} = 2\int_0^{Y_{\phi_i}} (X_w - X_i)\mathrm{d}Y \tag{19}$$

For convenience, a nondimensional mass flow rate parameter is defined as

$$\dot{m} = \frac{\text{mass flow rate}}{\rho_\infty V_\infty \ell_w^2} \tag{20}$$

One important point that should be stressed now is that we have assumed an infinitesimal thin inlet wall; therefore, its presence would not affect the flowfield, i.e., the flow will tend to move easily past the inlet without producing any disturbance.

Lift, Drag, and Geometric Variables

Lift and drag of the waverider configurations can be obtained by means of the integral momentum equations for inviscid flow. This process reduces the formulas for lift (L) and forebody wave drag (D_w), to area integrals over the shock-layer area between the body and shock in the base plane.

Recall that the waverider configuration with an integrated inlet is comprised of two surfaces—a waverider compression surface and an inlet compression surface. To calculate the lift and drag, the quantities associated with the original waverider forebody and inlet are summed together, then the amounts related to the overlapped portion of these two parts are deleted. The integral momentum equations are split into four parts; thereafter, the superposition method is applied to sum up the lift and drag of the whole configuration. The results are as follows (for details, see Ref. 5):

$$\begin{aligned} L = 4q\ell^2\delta^2\Bigg\{ & \int_{\phi_{i\ell}}^{\phi_\ell}\int_{\theta_{cb}}^{\beta} F1(\theta_o,\phi)\mathrm{d}\theta_o\mathrm{d}\phi \\ & + \int_0^{\phi_{i\ell}}\int_{\theta_{icb}}^{\beta} F1(\theta_o,\phi)\mathrm{d}\theta_o\mathrm{d}\phi \\ & + \left(\frac{r_i}{\ell}\right)^2\Bigg[\int_0^{\phi_i}\int_{\theta_{cb}}^{\beta} F1(\theta_o,\phi)\mathrm{d}\theta_o\mathrm{d}\phi \\ & - \int_0^{\phi_i}\int_{\theta_{icb}}^{\beta} F1(\theta_o,\phi)\mathrm{d}\theta_o\mathrm{d}\phi\Bigg]\Bigg\} \end{aligned} \tag{21}$$

$$\begin{aligned} D_w = 2q\ell^2\delta^2\Bigg\{ & \int_{\phi_{i\ell}}^{\phi_\ell}\int_{\theta_{cb}}^{\beta} F2(\theta_o,\phi)\mathrm{d}\theta_o\mathrm{d}\phi \\ & + \int_0^{\phi_{i\ell}}\int_{\theta_{icb}}^{\beta} F2(\theta_o,\phi)\mathrm{d}\theta_o\mathrm{d}\phi \\ & + \left(\frac{r_i}{\ell}\right)^2\Bigg[\int_0^{\phi_i}\int_{\theta_{cb}}^{\beta} F2(\theta_o,\phi)\mathrm{d}\theta_o\mathrm{d}\phi \\ & - \int_0^{\phi_i}\int_{\theta_{icb}}^{\beta} F2(\theta_o,\phi)\mathrm{d}\theta_o\mathrm{d}\phi\Bigg]\Bigg\} \end{aligned} \tag{22}$$

where

$$F1(\theta_o,\phi) = \frac{\rho(\beta)}{\rho_\infty}\cos(\phi) + \epsilon L^*_{mn}$$

$$F2(\theta_o,\phi) = \left[\frac{\rho(\beta)}{\rho_\infty}\left(2 + ln\frac{\beta^2}{\theta_o^2}\right) - \frac{C_{p_\ell}}{\delta^2} + \epsilon D^*_{mn}\cos(n\phi)\right]\theta_o$$

and

$$\begin{aligned} L^*_{mn} = & \left[\rho_{mn} + \frac{\mathrm{d}\theta_{mn}}{\mathrm{d}\theta_o} + \frac{\theta_{mn}}{\theta_o} + \frac{\theta_o}{\delta}\left(\frac{\theta_{mn}}{\delta} + \frac{V_{mn}}{V_\infty\delta}\right)\right] \\ & \times \cos(\phi)\cos(n\phi) - \frac{\theta_o}{\delta}\frac{W_{mn}}{V_\infty\delta}\sin(\phi)\sin(n\phi) \end{aligned}$$

$$\begin{aligned} D^*_{mn} = & \left[\frac{\rho_o}{\rho_\infty}\left(2 + ln\frac{\beta^2}{\theta_o^2}\right) - \frac{C_{p_\ell}}{2}\right]\left[\frac{\theta_{mn}}{\theta_o} + \frac{\mathrm{d}\theta_{mn}}{\mathrm{d}\theta_o}\right] \\ & + \frac{\rho_o}{\rho_\infty}\left[\rho_{mn}\left(2 + ln\frac{\beta^2}{\theta_o^2}\right) - 2\left(\frac{U_{mn}}{V_\infty\delta^2} - \frac{\theta_{mn}}{\theta_o}\right.\right. \\ & \left.\left. - 2\frac{V_{mn}}{V_\infty\delta}\frac{\theta_o}{\delta}\right)\right] - \frac{C_{p_{mn}}}{\delta^2} \end{aligned}$$

Here ϕ_s is the azimuthal angle of the particular cross section which is specified by $r/\ell = r_i/\ell$; and $\phi_{i\ell}$ represents the azimuthal angle of the inlet on the base plane. In calculations, $\phi_{i\ell}$ is usually approximated by ϕ_i.

The total drag is determined by

$$D = D_w + D_f + D_b \tag{23}$$

Here, D_w is the inviscid wave drag on the forebody. The friction drag D_f is represented by qC_fS_w, where S_w is the forebody wetted area and C_f an average skin-friction coefficient. As in Ref. 8, we choose $C_f = 0.001$ for the parametric study in the next section. The base drag D_b is ignored and set to zero in the subsequent analysis (this is tantamount to assuming that the base pressure is P_∞).

With regard to the total wetted area S_w of the forebody, it is determined by the geometry of the waverider and can be expressed as

$$S_w = S_{wf} + S_{wc} \tag{24}$$

where the freestream wetted area S_{wf} is specified as

$$S_{wf} = 2\ell^2\delta \int_0^{\phi_s} \sigma[1 - Z] \left[Z^2 + \frac{R_{cb}^2 R_{cb}'^2}{(R_{cb}^2 - 1)(\sigma^2 - 1)}\right]^{1/2} d\phi \tag{25}$$

and the compression wetted area S_{wc} is given by

$$\begin{aligned} S_{wc} = 2\ell^2\delta \Bigg[& \int_{\phi_{i\ell}}^{\phi_\ell} \int_Z^1 \left(\frac{R_{cb}^2 R_{cb}'^2}{R_{cb}^2 - 1 + X} + R_{cb}^2 - 1 + X^2\right)^{1/2} dX d\phi \\ & + \int_0^{\phi_{i\ell}} \int_{Z_i}^1 \left(\frac{R_{icb}^2 R_{icb}'^2}{R_{icb}^2 - 1 + X} + R_{icb}^2 - 1 + X^2\right)^{1/2} dX d\phi \\ & + \int_0^{\phi_i} \int_Z^{r_i/\ell} \left(\frac{R_{cb}^2 R_{cb}'^2}{R_{cb}^2 - 1 + X} + R_{cb}^2 - 1 + X^2\right)^{1/2} dX d\phi \\ & - \int_0^{\phi_i} \int_{Z_i}^{r_i/\ell} \left(\frac{R_{icb}^2 R_{icb}'^2}{R_{icb}^2 - 1 + X} + R_{icb}^2 - 1 + X^2\right)^{1/2} dX d\phi \Bigg] \end{aligned} \tag{26}$$

where

$$Z = \left(\frac{R_{cb}^2 - 1}{\sigma^2 - 1}\right)^{1/2}$$

$$Z_i = \left(\frac{R_{icb}^2 - 1}{\sigma^2 - 1}\right)^{1/2}$$

Parametric Analysis

Parametric analyses are performed to generate inlets and to determine the aerodynamic characteristics influenced by variations of inlet geometry and location. To illustrate the parametric study, a particular waverider configuration is considered; it is constructed of a fourth-order freestream trailing-edge curve with zero-slope edge and with the following design conditions: $M_\infty = 10$, $\delta = 8$ deg, $\phi_\ell = 50$ deg $R_0 = X_{\phi\ell}/2$, $m = 1$, $n = 2$, and $\epsilon = 0.1$. These types of waverider configurations have been extensively discussed in Ref. 9.

The previous section provides that three important parameters (R_{i0}, ϕ_i, r_i/ℓ) control the inlet shape. The influence of the parameters on the aerodynamic forces will be discussed in detail in the following subsections.

Influence of Parameter R_{i0}

The inlet thickness is controlled directly by R_{i0}, and increasing R_{i0} thickens the inlet. Moreover, the cross-sectional area of an inlet enlarges along with an increase in R_{i0}; it follows that the mass flow rate of the inlet also increases with R_{i0}, as shown in Fig. 4 for various parametric values of ϕ_i.

With regard to the influence on the aerodynamic forces, the pressure distribution inside the shock layer is examined for a hypersonic flow past a cone with combined transverse and longitudinal curvature. From Ref. 5, the pressure is greater at the body than at the shock. Thus, the increase of R_{i0} results in the pressure decrease on the inlet wall which will cause both the lift and the wave drag to decrease. Conversely, the wetted area enlarges as the inlet shape thickens; thus the friction drag D_f increases with R_{i0}. In summary, the lift decreases more than the drag, which produces a decrease in L/D as demonstrated in Fig. 5 for two values of ϕ_i.

Influence of Parameter ϕ_i

Azimuthal angle ϕ_i is the control parameter of the inlet width. Figures 6 and 7 indicate the cross-sectional area and mass flow rate of an inlet become larger as ϕ_i increases. With the same argument as described in the last section, the lift-to-drag ratio decreases monotonically as ϕ_i increases (see Fig. 8).

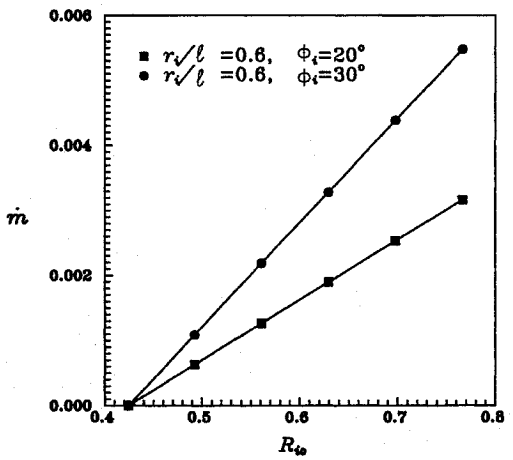

Fig. 4 Mass flow rate as function of R_{i0} for various values of ϕ_i.

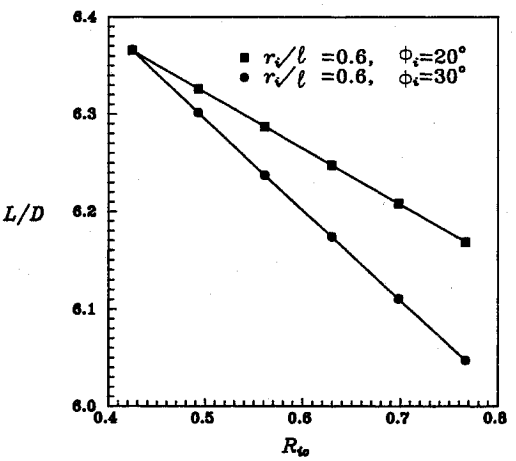

Fig. 5 Lift-to-drag ratio as function of R_{i0} for various values of ϕ_i.

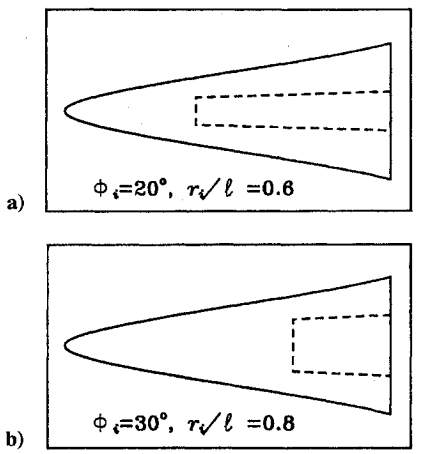

Fig. 6 Inlet configurations for different ϕ_i and r_i/ℓ.

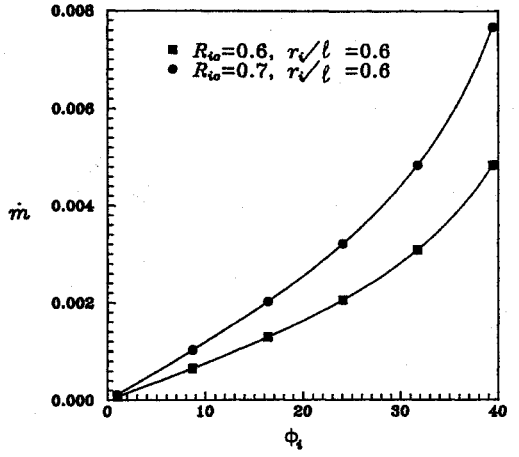

Fig. 7 Mass flow rate as a function of ϕ_i for various values of R_{i0}.

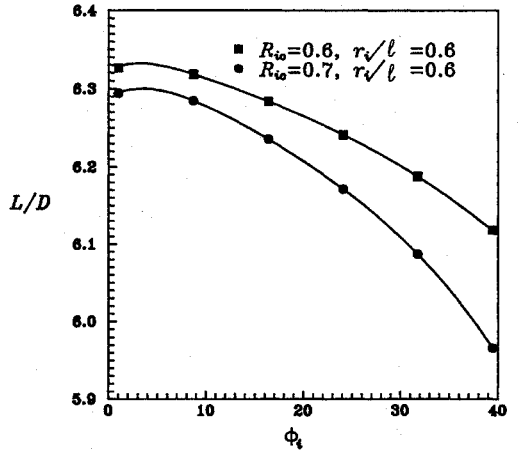

Fig. 8 Lift-to-drag ratio as a function of ϕ_i for various values of R_{i0}.

Length of Inlet

Figure 6 indicates that r_i/ℓ is the fraction parameter designed to control the inlet length. Only the portion of $(r/\ell) \geq (r_i/\ell)$ is related to the inlet wall; thus the inlet becomes shorter as r_i/ℓ increases. When r_i/ℓ reaches unity, the inlet unit disappears. From the foregoing discussion, the inlet portion can be treated as a stream tube; hence a constant mass flow rate is expected and is independent of the length of inlet. Therefore, the variation of r_i/ℓ would not change the mass flow rate of the inlet. However, an increase of r_i/ℓ causes a shorter inlet section which has smaller frictional drag. With the unchanged lift force, an increase in L/D is obtained for increasing r_i/ℓ. These results are demonstrated in Fig. 9 for various values of R_{i0}.

Concluding Remarks

By means of a simple and systematic scheme, the stream surface of the nonaxisymmetric hypersonic flowfield with longitudinal curvature has been utilized to design the waverider configuration with a smooth integrated inlet. This inlet is attached to the waverider configuration and is positioned to capture favorable flow into the engine; thus the design of the inlet for the scramjet is simplified. Also, the rate of mass flow through the inlets has been obtained in a closed form. Furthermore, the design scheme offers an explicit, approximate, and analytical form for both aerodynamic performance and geometric factors. This result can be used to perform a systematic and parametric study. The method established here can also be used to develop other waverider configurations with a bi-inlet, or even with vertical fins. The designer thus has at his disposal a systematic means for varying the large number of parameters which specify various flight conditions, forebody configurations and inlet configurations of hypersonic vehicles.

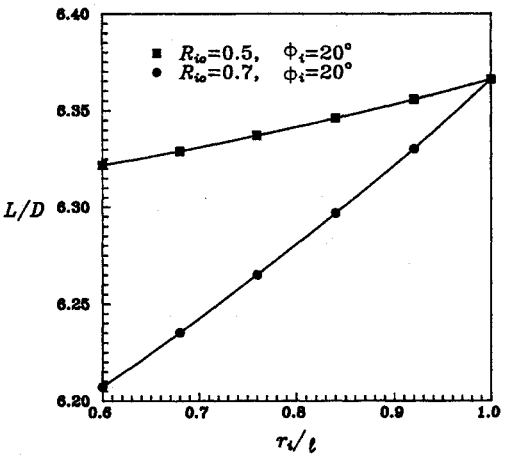

Fig. 9 Lift-to-drag ratio as a function of r_i/ℓ for various values of R_{i0}.

Acknowledgment

The financial support for this work from National Science Council Grant NSC 80-0401-E-011-05 is gratefully acknowledged.

References

[1] Kuchemann, D., "Hypersonic Aircraft and Their Aerodynamic Problems," *Progress in Aeronautical Sciences*, Vol. 6, Pergamon, London, 1965, p. 271.

[2] Nonweiler, T. R. F., "Aerodynamic Problems of Manned Space Vehicles," *Journal of the Royal Aeronautical Society*, Vol. 63, No. 585, 1959, pp. 521–528.

[3] Taylor, G. I., and Maccoll, J. W., "The Air Pressure on Cones Moving at High Speeds," *Proceedings of the Royal Society of London*, Series A, Vol. 139, 1933, pp. 278–311.

[4] Rasmussen, M. L., "Waverider Configurations Derived from Inclined Circular and Elliptic Cones," *Journal of Spacecraft and Rockets*, Vol. 17, No. 6, 1980, pp. 537–545.

[5] Lin, S. C., and Rasmussen, M. L., "Cone-Derived Waverider with Combined Transverse and Longitudinal Curvature," AIAA Paper 88-0371, Jan. 1988.

[6] Rasmussen, M. L., and He, X., "Analysis of Cone-Derived Waveriders by Hypersonic Small-Disturbance Theory," *NASA 1st International Hypersonic Waverider Symposium*, College Park, MD, Oct. 1990, pp. 1–46.

[7] Hemdan, H. T., and Jischke, M. C., "Inlets for Waveriders Derived from Elliptic-Cone Stream Surfaces," *Journal of Spacecraft and Rockets*, Vol. 24, No. 1, 1987, pp. 23–32.

[8] Rasmussen, M. L., and Stevens, D. R., "On Waverider Shapes Applied to Aero-Space Plane Forebody Configurations," AIAA Paper 87-2550, Aug. 1987.

[9] Lin, S. C., and Lu, S. C., "The Study of Hypersonic Waverider with Curvature," *Proceedings of the 8th National Conference of the Chinese Society of Mechanical Engineering*, Vol. 1, Taiwan, ROC, Nov. 1991, pp. 193–202.

[10] Kim, B. S., Rasmussen, M. L., and Jischke, M. C., "Optimization of Waverider Configurations Generated from Axisymmetric Conical Flows," AIAA Paper 82-1299, Aug. 1982.

Gerald T. Chrusciel
Associate Editor